LANGMUIR

pubs.acs.org/Langmuir Article

Programming Solitons in Liquid Crystals Using Surface Chemistry

Soumik Das, Sangchul Roh, Noe Atzin, Ali Mozaffari, Xingzhou Tang, Juan J. de Pablo, and Nicholas L. Abbott*

Cite This: *Langmuir* 2022, 38, 3575−3584 Read Online

ACCESS | Metrics & More | Article Recommendations | Supporting Information

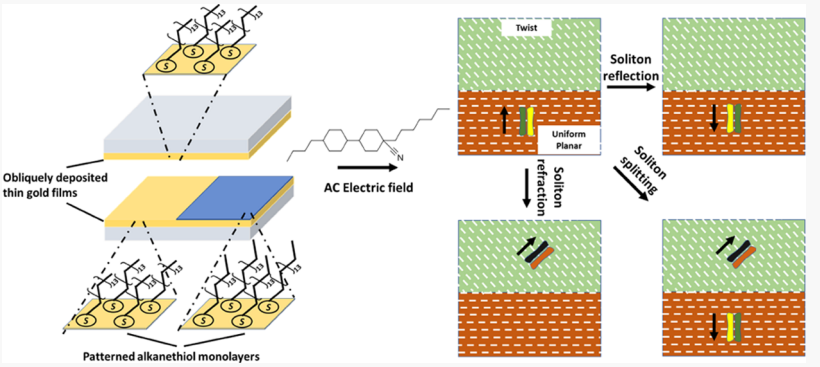

ABSTRACT: AC electric fields cause three-dimensional orientational fluctuations (solitons) to form and rapidly propagate in confined films of liquid crystals (LCs), offering the basis of a new class of active soft matter (e.g., for accelerating mixing and transport processes in microscale chemical systems). How surface chemistry impacts the formation and trajectories of solitons, however, is not understood. Here, we show that self-assembled monolayers (SAMs) formed from alkanethiols on gold, which permit precise control over surface chemistry, are electrochemically stable over voltage and frequency windows (<100 V; 1 kHz) that lead to soliton formation in achiral nematic films of 4′-butyl-4-heptyl-bicyclohexyl-4-carbonitrile (CCN-47). By comparing soliton formation in LC films confined by SAMs formed from hexadecanethiol ($C_{16}SH$) or pentadecanethiol ($C_{15}SH$), we reveal that the electric field required for soliton formation increases with the LC anchoring energy: surfaces patterned with regions of $C_{16}SH$ and $C_{15}SH$ SAMs thus permit spatially controlled creation and annihilation of solitons necessary to generate a net flux of solitons. We also show that solitons propagate in orthogonal directions when confined by obliquely deposited gold films decorated with SAMs formed from $C_{16}SH$ or $C_{15}SH$ and that the azimuthal direction of propagation of solitons within achiral LC films possessing surface-induced twists is not unique but reflects variation in the spatial location of the solitons across the thickness of the twisted LC film. Finally, discontinuous changes in LC orientation induced by patterned surface anchoring lead to a range of new soliton behaviors including refraction, reflection, and splitting of solitons at the domain boundaries. Overall, our results provide new approaches for the controlled generation and programming of solitons with complex and precise trajectories, principles that inform new designs of chemical soft matter.

INTRODUCTION

Solitons are spatially localized solitary waves that can travel long distances at constant speeds without losing their shape because nonlinear feedback during wave propagation minimizes broadening (dispersion) of the waves.[1,2] Solitons have been observed in a range of natural contexts, such as the propagation of waves of water along shallow canals, and they have been hypothesized to play a role in biological phenomena such as signal propagation along neurons.[3−5] Solitons have also been exploited in engineered systems, including for long-distance propagation of optical signals,[6−11] and they have been observed to form and propagate through in liquid crystals (LCs) as walls (localized regions of the LC in which the director reorients by 180°) in the presence of rotating magnetic fields.[12−17] More recently, solitons have been observed to form and/or propagate through nematic and cholesteric LCs in the presence of AC electric (and optical) fields[18−29] and used to transport colloidal microcargo.[23,24,27,30] Overall, these recent observations hint at the potential utility of solitons for programming rapid and long-distance transport of information and chemical species within LCs, capabilities that have the potential to be useful for designing adaptive and autonomous microscale LC-based chemical systems.[30−39]

Received: January 27, 2022
Revised: February 21, 2022
Published: March 9, 2022

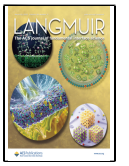

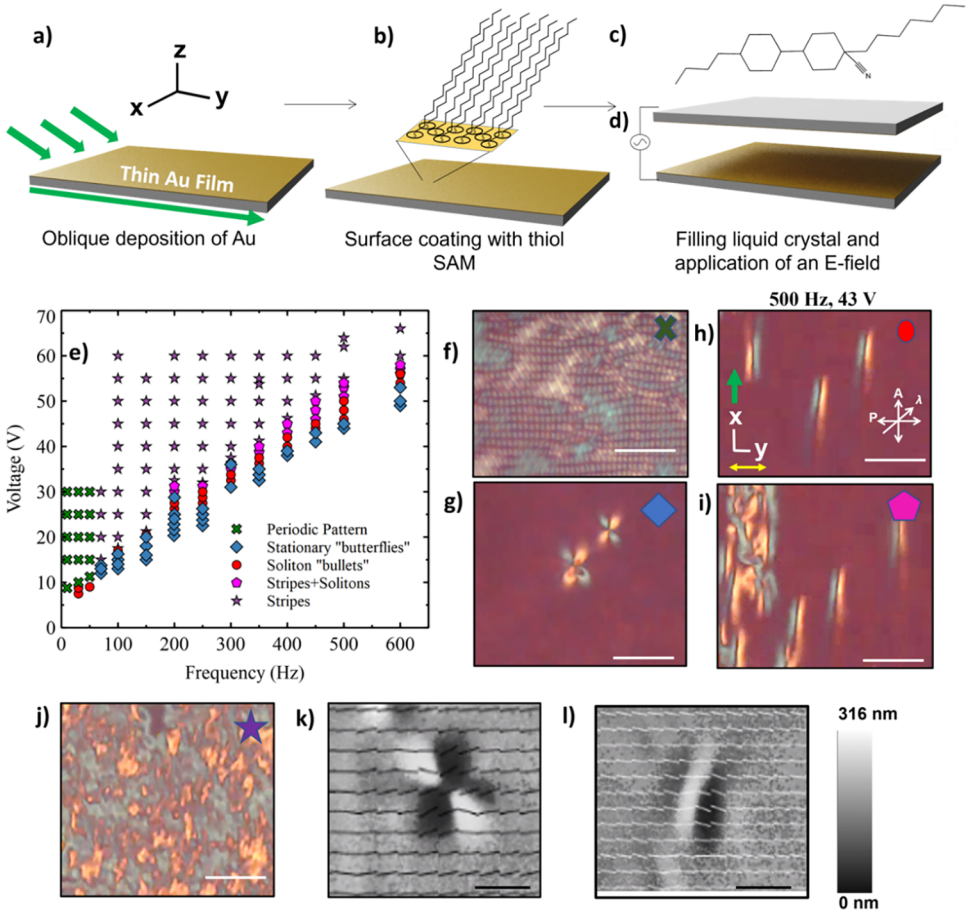

Figure 1. (a) Schematic illustration showing oblique deposition of gold onto a glass substrate. The green arrow indicates the direction of Au deposition. (b) Schematic illustrations of $C_{15}SH$ SAMs on gold films. (c) Molecular structure of the liquid crystal, CCN-47, used in this study. (d) Experimental setup used to generate solitons, comprising of an optical cell with SAM-coated surfaces, across which is applied an AC electric field. (e) Phase diagram as a function of electric voltage and frequency, depicting different states of director distortions in a sample cell of thickness 8 μm at 45 °C. (f) Low-frequency patterns, (g) stationary "butterflies," (h) "bullet" solitons, (i) solitons + stripes, and (j) stripes. Scale bars 50 μm. The surfaces confining the LC are $C_{15}SH$ SAMs. The phase diagram was obtained from the same sample. A variation of $\pm$1 V at each point was obtained across multiple (>10) samples. The green arrow in (h) indicates the direction of Au deposition. The LC alignment is indicated by the yellow double-headed arrow in (h). (k, l) Polscope images showing the LC orientations within a (k) stationary "butterfly" and (l) a traveling soliton. Scale bars 30 μm.

Solitons can be induced in LC systems with AC electric fields by applying the fields across micrometer-thick films of LCs that are confined between electrodes: surface interactions cause the LC to adopt orientations that are parallel to the electrode surfaces (planar surface anchoring of the LC). When using nematic LCs with $\Delta\varepsilon < 0$ and $\Delta\sigma < 0$, where $\Delta\varepsilon$ is the dielectric anisotropy and $\Delta\sigma$ is the anisotropy in ionic conductivity, the formation of solitons cannot arise from dielectric torques or electrohydrodynamic instabilities due to migration of ions in the LC (so-called Carr−Helfrich mechanism, which is applicable for $\Delta\sigma > 0$).[40] Instead, flexoelectric polarization has been proposed as the primary reason for the formation of the solitons.[19] This hypothesis is supported by the observation that solitons exhibit periodic director oscillations of the same frequency as the applied electric field ($f > 100$ kHz).[19] Although the addition of salts modifies soliton behaviors (in part due to electrohydrodynamic instabilities),[22,24,27] solitons are also observed in the absence of added electrolytes.[19,24]

In the studies described above, the initial alignment of the LC on the electrode surface (indium tin oxide (ITO)) was obtained using mechanically sheared polyimide films (PI-2555)[19,22,24] or photoaligned dyes.[24,27] While one study has hinted that weak LC anchoring is favorable for solitons generated in the presence of electrohydrodynamic instabilities,[27] the influence of surface interactions on soliton formation in LCs has not been explored in detail nor is it fully understood. Because soliton formation involves a localized perturbation of the LC orientation away from the surface-induced orientation of the LC film, we hypothesized that surface interactions may play an important role in both soliton formation and propagation. In this work, we explore the effects of LC surface interactions on solitons using a class of surfaces, self-assembled monolayers (SAMs) formed from alkanethiols on thin gold films that allow precise and versatile control over the anchoring of LCs, including patterned anchoring of LCs.[41−43] We further demonstrate that control over LC surface anchoring enables spatially localized soliton formation and precise programming of soliton trajectories (e.g., refraction, reflection) at the boundaries of LC orientational domains.

Our study focuses on three key issues. First, we address the question of whether the LC anchoring strength (anchoring energy density) influences the frequency and magnitude of the electric field needed to form solitons in LCs. We focus on LCs with $\Delta\varepsilon < 0$ and $\Delta\sigma < 0$ to avoid the additional complexity of electrohydrodynamic instabilities.[40] Second, we investigate how surface-induced strain within an LC, in the form of a twist in

https://doi.org/10.1021/acs.langmuir.2c00231
Langmuir 2022, 38, 3575−3584

azimuthal orientation across the thickness of an LC film, impacts soliton formation and motion. While past studies have explored soliton formation in cholesteric LCs (where the presence of a twist corresponds to the ground state[24]), the influence of elastic strain within LCs on soliton formation and propagation has not been explored. Third, we explore soliton behaviors in LC systems with patterned surface anchoring, with a focus on surfaces patterned with distinct anchoring energies and discontinuous changes in LC orientations. Past studies have observed that boundaries such as electrode edges can be sources of solitons[19] and that continuous changes in LC orientation can guide soliton trajectories.[24] In contrast, as detailed below, we find that discontinuous changes in LC orientation can generate new soliton behaviors, including their creation, annihilation, splitting, reflection, and refraction. Overall, our results illustrate how patterned surfaces can be used to program complex soliton trajectories.

RESULTS

SAMs Formed from Pentadecanethiol (C_{15}SH) and Hexadecanethiol (C_{16}SH). In our first experiments, we sought to determine the influence of LC surface anchoring energy on the generation of solitons using SAMs formed from alkanethiols on obliquely deposited thin films of gold. The structures of SAMs formed from alkanethiols have been extensively characterized, revealing that they form quasi-two-dimensional crystals in which the aliphatic chains remain in an all trans configuration with the terminal methyl groups presented in well-defined orientations (which differ for alkanethiols with odd and even numbers of carbons).[41,42] Past studies have established that the choice of the alkanethiol used to form a SAM can influence the orientation of LCs anchored on SAMs.[41,42,44−47] Specifically, alkanethiols with odd and even numbers of carbons both cause nematic films of 4-cyano-4′-pentylbiphenyl (5CB) to adopt a planar orientation, but with an azimuthal direction that is either parallel (even number of carbons) or perpendicular (odd number of carbons) to the direction of deposition of the gold film.[41,42] This so-called odd−even anchoring behavior arises from competing influences of the nanometer-scale topography of the polycrystalline gold film (which orients the LC in the direction of minimum surface roughness)[41,42,47] and the molecular organization of the SAMs (which orients the LC through interactions with the terminal methyl groups of the SAMs).[41,42,47] The use of odd or even chain-length alkanethiol SAMs thus allowed us to investigate how changes in the surface anchoring of LCs impact the formation and propagation of solitons.

Prior observations of the orientations of LCs on SAMs formed from alkanethiols used LCs such as 5CB, which have molecular structures and physical properties that differ substantially from CCN-47 used in the current investigation. In particular, 5CB forms a room temperature nematic phase, whereas the experiments with nematic phases of CCN-47 are necessarily performed at elevated temperatures (CCN-47 forms a nematic phase between 30.6 and 59.7 °C), with elevated temperatures potentially influencing the organization and stability of SAMs.[48−51] Accordingly, we first determined if it was possible to orient nematic phases of CCN-47 at 45 °C when supported on SAMs formed from alkanethiols on obliquely deposited gold films. Figure 1a shows a schematic illustration of the physical vapor deposition of gold at an oblique angle of incidence to form a thin gold film (Figure 1b; direction of gold deposition is shown in green arrows in Figure 1a). The optical cells (Figure 1d) used in our study were prepared from the semitransparent gold films. Detailed experimental methods can be found in the Supporting Information (SI). Using optical microscopy (transmission mode; crossed polarizers), we determined that the nematic phase of CCN-47 at 45 °C (Figure 1c) does adopt a uniform azimuthal orientation on C_{15}SH SAMs, and that the azimuthal orientation of the LC is orthogonal to the direction of deposition of the gold used to form the gold film. This orientation is similar to 5CB, consistent with prior conclusions that the nanoscale roughness of the gold films dominates the orientation of LCs on SAMs formed from alkanethiols with odd number of carbons (minimization of the elastic energy on the rough surface causes 5CB and CCN-47 to adopt the same orientation).[41,42,47]

Next, we examined whether solitons form when nematic phases of CCN-47 are confined by SAMs formed from C_{15}SH. At the onset of these experiments, it was not obvious to us that SAMs would permit generation of solitons because the anchoring energies of CCN-47 on the SAMs were not known (5CB has been reported previously to have an anchoring energy on a SAM of ∼30 $\mu J/m^2$)[52,53] and because SAMs formed from alkanethiols undergo electrochemical desorption from gold surfaces[54,55] (we considered it possible that the electric fields required to form solitons would damage and thus change the LC anchoring). Inspection of Figure 1h reveals that films of nematic CCN-47 with thicknesses of 8 μm, when confined by SAMs formed from C_{15}SH, do exhibit localized LC director perturbations that are consistent with soliton formation and propagation across the sample when an AC electric field with a frequency of 500 Hz and voltage of 43 V is applied across the LC. Similar to prior reports of soliton formation on PI surfaces at high frequencies (>100 Hz),[19] we observed the solitons to propagate in a direction perpendicular to the LC director (independent of the strength of applied electric field). We also found that SAMs could be used multiple times over a period of a week to reproducibly generate solitons. Overall, these results provide the first evidence that alkanethiol SAMs are sufficiently stable electrochemically to allow the generation of solitons.

As noted above, previous reports have revealed that solitons form over narrow ranges of electric field strengths, influenced by factors such as temperature, LC film thickness, LC elastic constants, and the presence or absence of salts.[19,22,24] To elucidate the role of surface interactions on soliton generation, and to define the conditions under which solitons form in our experimental system, we varied the frequency and voltage in sample cells prepared with C_{15}SH SAMs. A phase diagram describing the different director morphologies at 45 °C, as a function of frequency and voltage, for 8 μm thick LC films prepared with C_{15}SH SAMs, is shown in Figure 1e. Overall, this phase diagram exhibits many features similar to those reported with PI surfaces.[19] Specifically, at low frequencies (<80 Hz), periodic patterns formed in the LC (Figure 1f), similar to electrohydrodynamic convection patterns.[56] Beyond this frequency, with increasing voltage, we first observed stationary director distortions in the shape of a butterfly (Figure 1g, i.e., with quadrupolar symmetry with four lobes). The butterfly structures, which tended to form around particles (Figure S3) or imperfections on the surfaces (Figure S4),[19] were often observed to serve as sites for the nucleation of propagating solitons (Figure S5), with propagating solitons generated at voltages above those at which butterflies were formed. We used a Polscope (see the SI for details) to obtain the LC director profiles within the stationary butterflies (Figure 1k) and the propagating solitons (Figure 1l). The images obtained using the

https://doi.org/10.1021/acs.langmuir.2c00231
Langmuir 2022, 38, 3575−3584

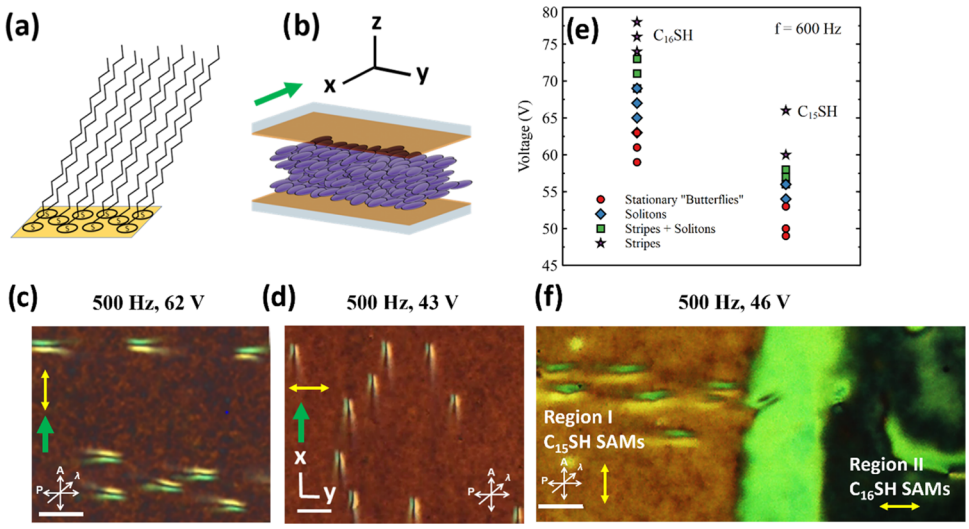

Figure 2. (a) Schematic illustration of a $C_{16}SH$ SAM on a gold film. (b) Schematic illustration of the LC orientation when confined by two surfaces decorated with $C_{16}SH$ SAMs. (c,d) Traveling solitons observed in optical cells formed using $C_{16}SH$ and $C_{15}SH$ SAMs, respectively (thickness: 8 μm, temperature: 45 °C). Green arrows indicate the direction of Au deposition. The LC alignment is indicated by the yellow double-headed arrow in (c) and (d). (e) Electric voltages required to generate different LC director distortions in samples made with $C_{16}SH$ SAMs (left) and $C_{15}SH$ SAMs (right) (frequency: 600 Hz, temperature: 45 °C, sample cell thickness: 8 μm). The electric voltage values were obtained from a single sample cell of each type. A variation of ±1 V at each point was obtained across multiple (>5) samples. (f) Soliton generation in cells patterned with $C_{16}SH$ and $C_{15}SH$ SAMs: Region I and Region II correspond to $C_{15}SH$ and $C_{16}SH$ SAMs, respectively. At 500 Hz and 46 V, solitons were only generated in Region I. Scale bars 50 μm.

Polscope confirmed the quadrupolar and bipolar symmetries of the LC within these two structures, respectively. The solitons propagated at velocities of 400−500 μm/s and the velocities increased with an increase in applied voltage (Figure S6). At a given frequency, solitons were observed over a narrow range of voltages (ΔV = 2−4 V), with solitons replaced by stripes at higher voltages (Figure 1i,j). Unlike the periodic patterns observed at low frequencies (Figure 1f), the stripes were irregular distortions that filled the entire LC sample cell. They also lacked the symmetry associated with the butterflies and moving solitons. Although the solitons formed using LC films confined by SAMs share many similarities with those reported previously using LCs confined by PI surfaces,[19] when compared to PI surfaces, the voltages required to generate solitons (at a given frequency, temperature, and sample cell thickness) in LC films confined by $C_{15}SH$ SAMs are lower ($V_{PI} - V_{thiol} \sim 5-8$ V).[19] This difference likely arises from differences in the magnitude of LC anchoring energy on the two types of surfaces (for 5CB, the azimuthal anchoring energies are ∼30 and ∼100 $\mu J/m^2$ for alkanethiol SAMs and PI, respectively),[57−59] a proposal that we explore below with CCN-47 by comparing anchoring energies and solitons obtained using two different SAMs.

We explored the effects of a change in LC anchoring on soliton formation by preparing SAMs from $C_{16}SH$ (Figure 2a) and comparing the results to those reported above using SAMs formed from $C_{15}SH$. This comparison led to two key observations. First, we measured the azimuthal orientation of the nematic CCN-47 film on a SAM formed from $C_{16}SH$ to be orthogonal to the orientation observed on the SAMs formed from $C_{15}SH$ (the azimuthal orientation of the LC on the SAM formed from $C_{16}SH$ was parallel to the direction of deposition of the gold film supporting the SAM (Figures 2b and S2)). This difference in orientation caused solitons in LCs confined by $C_{16}SH$ SAMs to travel in a direction orthogonal to the ones anchored by $C_{15}SH$ SAMs (Figure 2c). Second, at the same frequency, we measured the electric field required to generate solitons to be higher for the surfaces formed from $C_{16}SH$ SAMs (Figure 2e) than from SAMs formed from $C_{15}SH$ (65 ± 1 vs 53 ± 1 V, respectively, at 600 Hz). To understand the origins of this difference, we measured the azimuthal anchoring energies of CCN-47 on the two SAMs using methods described previously in the literature[52] and found them to be 0.72 ± 0.1 and 1.04 ± 0.13 $\mu J/m^2$ for $C_{15}SH$ and $C_{16}SH$ surfaces, respectively (using a Student's *t*-test, we found the two values differ from each other with a confidence level greater than 95%). Because the ratio of azimuthal to out-of-plane anchoring energy can be predicted from the ratio of Frank elastic constants of an LC (K_1/K_2),[60] we interpret our measurements to indicate that the out-of-plane anchoring energies of CCN-47 on $C_{15}SH$ and $C_{16}SH$ SAMs are 3 ± 0.4 and 4.3 ± 0.5 $\mu J/m^2$ respectively.[61] This result leads us to propose that the higher electric field required to generate solitons in LCs confined by $C_{16}SH$ SAMs arises from the stronger LC anchoring on these surfaces (as compared to $C_{15}SH$ SAMs).

The results above led us to ask if the formation of solitons can be constrained to occur at a specific spatial location using an LC sample with patterned anchoring energies. As shown in Figure 2f, using a sample patterned with $C_{15}SH$ and $C_{16}SH$ SAMs, we indeed observed that solitons appeared first in Region I (low anchoring energy) where both the confining surfaces are decorated by $C_{15}SH$ SAMs, relative to Region II with confining surfaces containing $C_{16}SH$ SAMs (high anchoring energy). We also observed that solitons generated in Region I were annihilated when they reached the boundary to Region II. Thus, we conclude that patterned SAMs can lead to spatially localized soliton generation and annihilation based on the local surface anchoring of the LC. Below we show that this phenomenon can lead to the creation of a net flux of solitons across the boundary between LC domains with distinct LC alignments. This result is an interesting one as past studies have

https://doi.org/10.1021/acs.langmuir.2c00231
Langmuir 2022, 38, 3575−3584

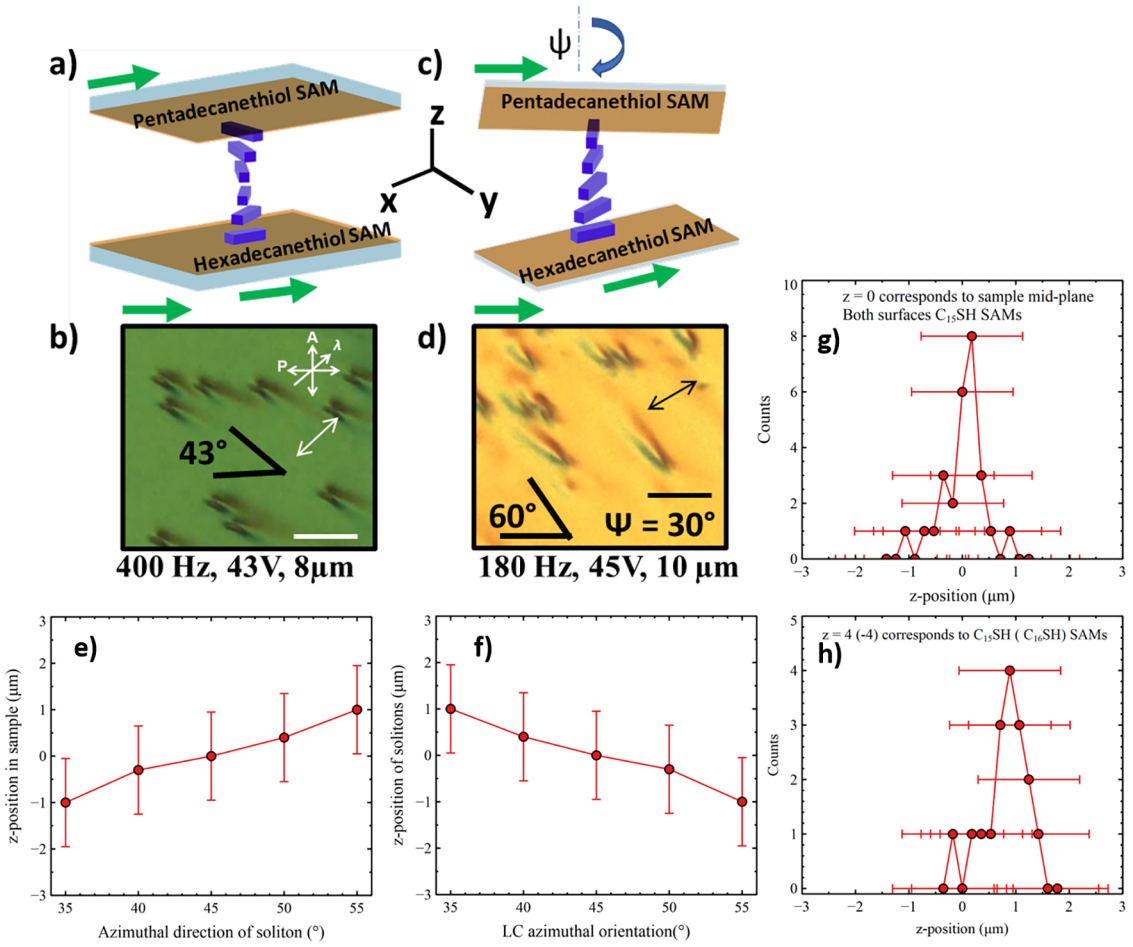

Figure 3. (a, c) Schematic illustration of twisted LC configurations generated with different mutual orientations of alkanethiol-decorated gold surfaces. (c) $\psi = 0°$ and (e) $\psi = 30°$ (clockwise). (b, d) Solitons generated in optical cells prepared as in (a) and (c) ($T = 45$ °C). The sample thicknesses in (b) and (d) were 8 and 10 μm, respectively. The double arrows indicate the director orientation at the sample midplane. Scale bars 50 μm. (e) z-position of solitons plotted against the azimuthal direction of soliton (measured anticlockwise from the y-axis) propagation in a twisted LC sample. The sample thickness was 8 μm. $z = 0$ corresponds to the midplane of the cell. (f) z-positions of propagating solitons plotted against the local LC azimuthal orientation. (g, h) Histogram plots showing the number of solitons at different z-positions across a sample in which the LC film is confined by (g) $C_{15}SH$ SAMs and (h) $C_{15}SH$ and $C_{16}SH$ SAMs, respectively. Here, $z = 0$ corresponds to the midplane of the sample. $z = 4(-4)$ corresponds to $C_{15}SH$ ($C_{16}SH$) SAMs in (h). The counts were obtained from a single snapshot over an area of $\sim 3 \times 10^5$ μm^2.

revealed that LC anchoring energies can be tuned by changing the terminal functional groups of SAMs.[52,62,63]

Solitons in Twisted Nematic LCs. The experiments reported in the previous sections demonstrate that solitons can be formed in LC films confined by gold surfaces decorated with alkanethiol SAMs. Next, we used this capability to induce twist distortions in LC thin films via surface interactions and to explore the influence of LC strain on soliton formation and propagation. Past studies have explored solitons in twisted LCs, but the prior studies used cholesteric LCs in which the twisted state is the ground state.[24] We investigated nematic LCs twisted via surface interactions for two reasons. First, we wanted to determine if solitons can form and propagate in the presence of a strain (i.e., a continuously varying azimuthal orientation across the LC sample) and, if they do form, determine whether the electric field magnitude and frequency required to form solitons differ from unstrained LC films. Second, we wanted to characterize the direction of propagation of solitons in LCs with surface-induced twists along with the locations of the corresponding solitons within the twisted LC structure. In the first set of experiments, the LCs were confined between two gold films decorated with $C_{15}SH$ SAMs, where the direction of gold deposition within each film was orthogonal (Figure S7). With the LC anchored in orthogonal azimuthal orientations on the two confining surfaces, the twist of the LC was determined by a competition between the bulk LC elastic energy (in the twisted LC state) and the LC anchoring energy (at the confining surfaces). We determined the twist in the LC samples in our experiments to be $88 \pm 2°$ using optical microscopy (see the SI for optical characterization). When an electric field (e.g., 500 Hz, 46 V) was applied across the sample, we observed the formation of propagating solitons (Figure S9), with no significant difference in the electric field conditions (53 ± 1 vs 52.5 ± 1 V at 600 Hz) required to form solitons in the twisted LC sample as compared to a uniformly oriented sample ($C_{15}SH$ SAMs) (Figure S10a). We also generated twisted LC samples by replacing one of the $C_{15}SH$ SAMs with a $C_{16}SH$ SAM (Figure 3a). Under these conditions, we found that a higher voltage ($\Delta V \sim 2$V) was required (at the same frequency) to generate propagating solitons, as compared to the case when the twist was generated by two $C_{15}SH$ SAMs (Figures 3b and S10b). We attribute this result to the high anchoring energy of the LC on the $C_{16}SH$ SAM. Overall, these results reveal that the presence of twist within the LC, when created by confining surfaces with

https://doi.org/10.1021/acs.langmuir.2c00231
Langmuir 2022, 38, 3575−3584

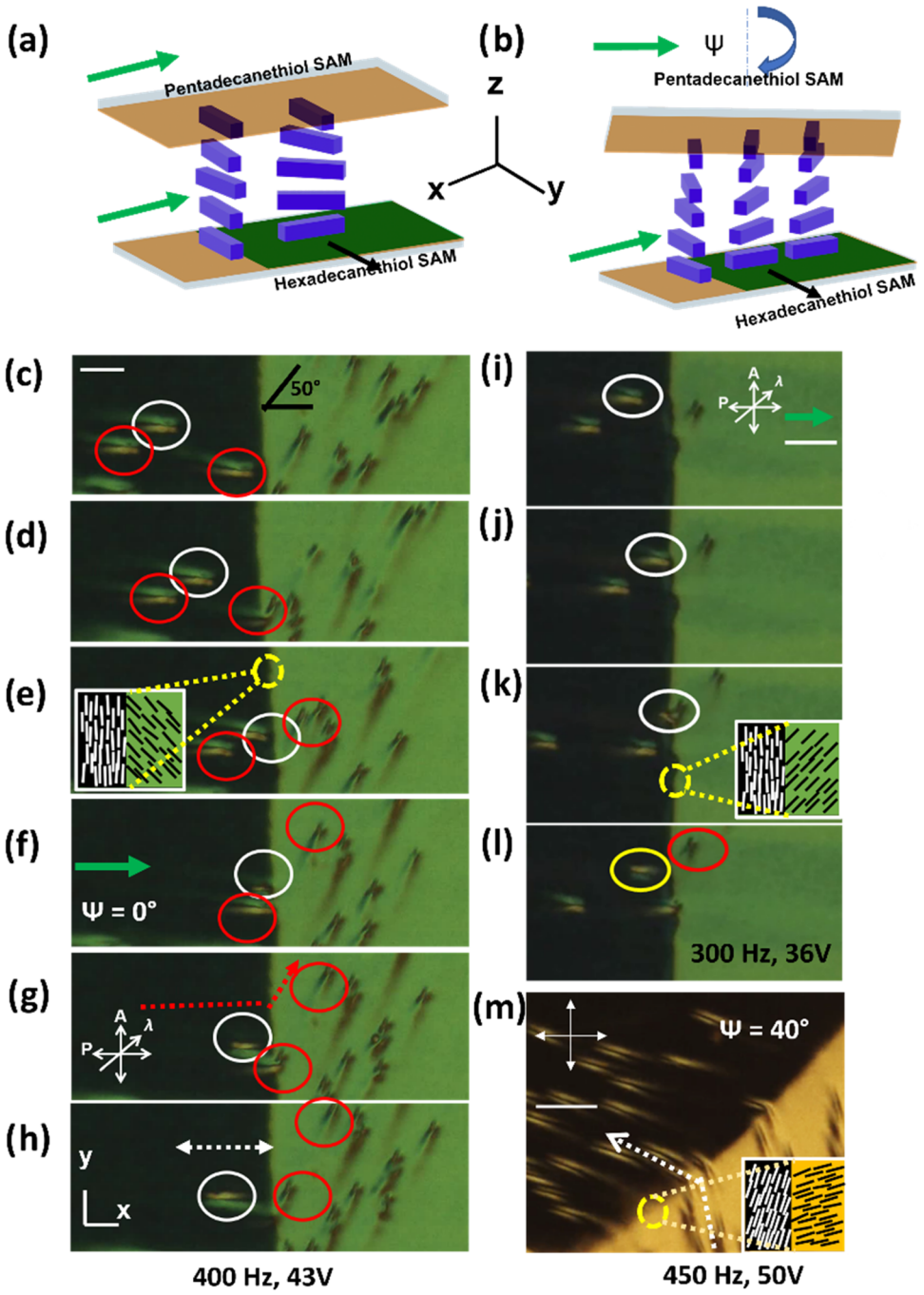

Figure 4. (a, b) Schematic illustration of LC alignment in optical cells patterned with SAMs to create uniform and twisted regions. The top surface in (b) is rotated by ψ to create patterned LC regions of two different twists. (c) Crossed polar images of LC textures in cells made of patterned SAMs. The dark and bright regions correspond to uniform (C_{15}SH SAMs) and twisted LC alignments, respectively. (c–h) Timed snapshots (0.1 s apart) showing trajectories of a soliton before and after encountering the boundary between LC domains with uniform and twisted director alignments (400 Hz, 43 V). The soliton circled in white reverses its direction at the interface. Solitons marked in red deviate in their direction of propagation by approximately 50° when crossing from a region of LC with uniform alignment to a twisted LC alignment. Green arrows indicate the direction of gold deposition (cell thickness = 8 μm, T = 45 °C). (i–l) Timed snapshots (0.2 s apart) showing the splitting of solitons at the boundary of two distinct LC alignments. The soliton circled in yellow reverses its direction at the interface and the soliton encircled in red moves to Region II with a change in trajectory direction of approximately 50° (f = 300 Hz; V = 36 V). (m) Trajectory of a soliton in an LC optical cell with patterned surfaces. The top surface of the cell is rotated by 40°. The director alignments near the boundary at the sample midplane are indicated in the insets of (e) and (m). Scale bars 50 μm.

identical SAMs, does not have a measurable effect on the conditions under which solitons form. Instead, the anchoring energy of the confining surfaces appears to dominate over the formation of the solitons.

Whereas uniformly oriented LC films generate solitons that propagate perpendicular (Figure 2c) or parallel (Figure 2d) to the direction of gold deposition, we found that solitons in twisted samples propagated over a distribution of angles (e.g., 35–55°, as shown in Figure 3a) rotated from the direction of gold deposition. We hypothesized that the soliton trajectories in the twisted cells are guided by the local LC azimuthal orientation within the x–y plane of the twisted LC sample in which the

https://doi.org/10.1021/acs.langmuir.2c00231
Langmuir 2022, 38, 3575–3584

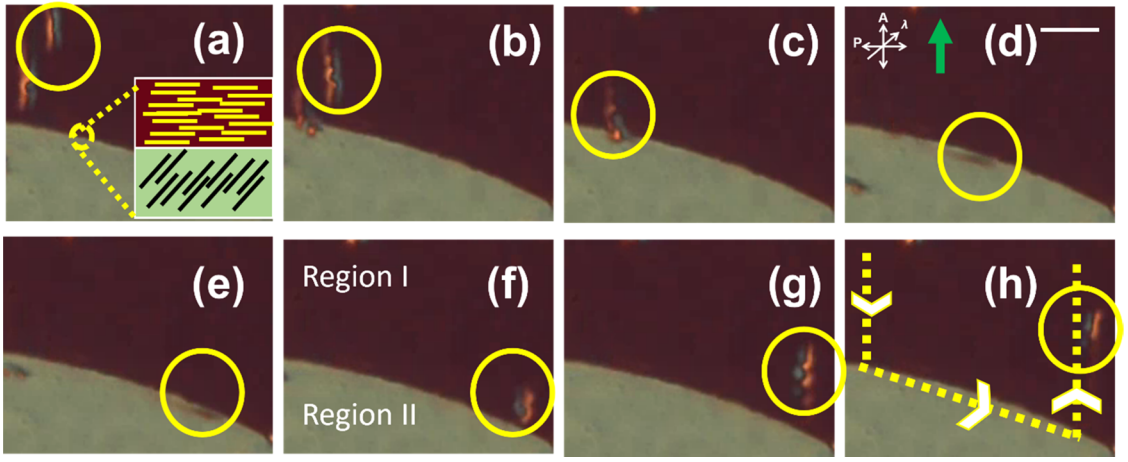

Figure 5. Optical micrographs of a soliton that exhibits a complex U-shaped trajectory in a spatially patterned optical cell. The dark region (Region I) corresponds to a uniform planar LC alignment on $C_{15}SH$ SAMs. The bright region (Region II) corresponds to twisted LC alignment between $C_{15}SH$ and $C_{16}SH$ SAMs. The soliton takes a U-turn, depicted by the yellow dotted line in (h), as it moves from Region I to Region II and back to Region I. The director alignments near the boundary at the midplane of the optical cell is illustrated in the inset of (a). The direction of gold deposition is indicated by the green arrow in (d). The soliton is indicated by the yellow circles (500 Hz, 51 V). Images are taken 0.1 s apart from each other. Scale bar 50 μm.

solitons propagate. To confirm this proposal, we calibrated the notches of the fine focus of our optical microscope to obtain the z-position of different solitons propagating through a twisted LC sample (Figure 3e). We observed a strong linear correlation between the z-position of the propagating solitons and the local azimuthal direction of propagation of solitons (Figure 3f). An alternative perspective on this result is that the direction of propagation of solitons in a twisted cell can be used to locate the z-position of the solitons. When the two SAMs used to generate the twisted state of the LC were identical (both $C_{15}SH$ SAMs), the majority of solitons were found to be localized near the midplane of the cell (Figure 3g), where the effect of surface anchoring on electric field-induced strain is minimized. However, when the LC was twisted using asymmetric surfaces (a $C_{16}SH$ and a $C_{15}SH$ SAM), the solitons were found to be located closer to the SAM formed from $C_{15}SH$ (Figure 3h), which possesses the weaker anchoring energy of the two SAMs (see above). Overall, this result provides further support for our previous conclusion that surface anchoring plays a key role in soliton formation and propagation. Our results indicate that twisted LC samples can be used to program soliton trajectories as the direction of propagation of the solitons can be controlled by either varying the SAM anchoring energy and/or varying the mutual orientations (ψ) of the confining gold surfaces (Figure 3c,d).

Solitons in Patterned LCs. Past studies have used photoaligned LCs to explore how continuous changes in LC alignment influence soliton trajectories.[24] Here, we examine the role of discontinuous domain boundaries on soliton behaviors by leveraging the capacity to pattern alkanethiol SAMs on gold surfaces to generate regions of distinct LC anchoring (see the SI for details).[43,64] Figure 4a shows a schematic illustration of an LC sample with patterned azimuthal alignment (see inset of Figure 4d). Since the two regions in the LC sample have distinct anchoring energies, consistent with the results reported above, with increasing voltage, we observed solitons to be generated preferentially in Region I, where both the confining surfaces were decorated by $C_{15}SH$ SAMs (Figure S12). Inspection of Figure 4c–h reveals that a set of solitons initially in Region I travel in a horizontal direction, which is perpendicular to the LC alignment in that region. When the solitons pass across the boundary with Region II, they change their direction of propagation to an angle that is approximately 50° from the direction of gold deposition (red dotted circles and red arrows in Figure 4c–h). This direction of soliton propagation is governed by the LC alignment in Region II. We observed that a majority of the solitons (~98%) exhibit this "refraction"-type behavior at the boundary between Region I and II. A small fraction of the solitons (<2%), however, were observed to be "reflected" by the interface (shown in white circles and white arrows in Figure 4c–h). We performed several experiments to elucidate what factors determined the distinct behaviors of the solitons observed at the domain boundaries. We considered the possibility that differences in the structure of the LC along the domain boundary underlie the distinct soliton behaviors. If boundary structural differences determined soliton behaviors, we would expect that soliton behavior would correlate strongly with location on the domain boundary. However, we did not observe solitons to be reflected at well-defined locations along the boundary of Region I and Region II (Figure S12). In contrast, we observed solitons being refracted at the same locations, along the boundary, where a different soliton was previously reflected (Figure S13). We propose that the instantaneous phase of the LC director inside the soliton, which oscillates with the applied electric field, at the time that it encounters the strained LC director at the domain boundary determines whether the soliton will refract or reflect at the domain boundary.

We also observed a small population (<1%) of propagating solitons to generate two solitons, one refracting and another reflecting, at the domain boundary (Figure 4i–l). While stationary solitons have been observed to split into two propagating solitons, and four solitons have been observed to form from the collision of two solitons,[24] the factors that trigger splitting in both contexts have not been identified. Our results indicate that boundaries that separate two LC regions with distinct orientations can trigger the splitting of a single propagating soliton. Along with refraction, reflection, splitting, and annihilation of solitons at domain boundaries, we also observed that solitons can be created at boundaries (Figure S14). These observations provide support for the proposal that

https://doi.org/10.1021/acs.langmuir.2c00231
Langmuir 2022, 38, 3575−3584

strained LCs present at the boundaries of LC domains with distinct alignments can lead to soliton behaviors not seen in systems where there is a continuous change in LC alignment.

We also prepared LC optical cells from two gold surfaces that were patterned with $C_{15}SH$ and $C_{16}SH$ SAMs and rotated relative to each other by an angle ψ (Figure 4b). This leads to adjacent LC domains that possess distinct magnitudes of twist (determined by ψ; see the inset of Figure 4m). We observed that we could tune soliton trajectories by varying the extent of ψ (Figure 4c,m). Furthermore, by varying the shape (curvature) of the boundary between two LC domains, we observed that it was possible for solitons to undergo multiple interactions with the boundary. In the example shown in Figure 5, we observed multiple interactions to cause the soliton to undergo a "U-turn." Overall, these experiments reveal that patterned LCs, and the behaviors of solitons at the discontinuous boundaries of the patterned domains, can lead to a complex and diverse range of soliton trajectories. These results demonstrate that patterned LCs can be used to spatially program the behaviors of solitons in ways that appear promising for the design of LC-based active matter.[23,30,36]

CONCLUSIONS

Overall, this work advances our understanding of the role of surface chemistry on soliton formation and propagation in LC films. We confined LC films between SAMs formed on obliquely deposited thin gold films and, in doing so, unmasked how LC surface interactions can impact soliton generation and direction of propagation. We found that the anchoring energy of the LC on the SAMs substantially influences the electric fields required to generate solitons. This result permitted spatial control over soliton generation and also provided insight into the locations at which solitons propagate in twisted LC films. We further demonstrate how patterned anchoring of LCs provides additional control over soliton formation and trajectories via the complex behaviors of solitons at discontinuous LC domain boundaries. The results in this study lead to the identification of several future directions of investigation, including the exploration of how a wider range of terminal chemical functional groups of SAMs influence solitons. Additionally, studies based on simulations have the potential to provide insight into the microscopic factors that control the reflection, refraction, generation, splitting, and destruction of solitons at boundaries between patterned LC domains. We also envisage future studies in which soliton trajectories are engineered in LCs to promote transport processes in microscale chemical systems (e.g., for materials synthesis or assembly).

ASSOCIATED CONTENT

Supporting Information

The Supporting Information is available free of charge at https://pubs.acs.org/doi/10.1021/acs.langmuir.2c00231.

Preparation of obliquely deposited thin films of gold; preparation of alkanethiol SAMs on gold surfaces; characterization of the orientations of LC confined between SAMs; observation of stationary butterflies near particles and surface imperfections; emission of solitons from stationary butterflies; velocity of solitons as a function of electric field strength; measurement of twist; propagating solitons in twisted LCs; electric field required to generate solitons in twisted LCs; preparation of patterned SAMs; and soliton behavior in patterned systems—spatially localized solitons, reflection, and creation of solitons (PDF)

AUTHOR INFORMATION

Corresponding Author

Nicholas L. Abbott − *Smith School of Chemical and Biomolecular Engineering, Cornell University, Ithaca, New York 14853, United States;* orcid.org/0000-0002-9653-0326; Email: nabbott@cornell.edu

Authors

Soumik Das − *Smith School of Chemical and Biomolecular Engineering, Cornell University, Ithaca, New York 14853, United States*

Sangchul Roh − *Smith School of Chemical and Biomolecular Engineering, Cornell University, Ithaca, New York 14853, United States*

Noe Atzin − *Pritzker School of Molecular Engineering, University of Chicago, Chicago, Illinois 60637, United States*

Ali Mozaffari − *Pritzker School of Molecular Engineering, University of Chicago, Chicago, Illinois 60637, United States; Center for Molecular Engineering, Argonne National Laboratory, Lemont, Illinois 60439, United States*

Xingzhou Tang − *Pritzker School of Molecular Engineering, University of Chicago, Chicago, Illinois 60637, United States*

Juan J. de Pablo − *Pritzker School of Molecular Engineering, University of Chicago, Chicago, Illinois 60637, United States;* orcid.org/0000-0002-3526-516X

Complete contact information is available at: https://pubs.acs.org/10.1021/acs.langmuir.2c00231

Author Contributions

S.D. and S.R. performed the experiments reported in this manuscript. N.A., A.M., and X.T. contributed to the analysis of the experiments. All authors drafted and edited the manuscript and have given approval to the final version of the manuscript.

Funding

The experiments reported in this paper were supported by the Department of Energy, Basic Energy Sciences, Division of Materials Research, Biomaterials Program under grant no. DE-SC0019762. This work made use of the Cornell Center for Materials Research Shared Facilities, which are supported through the NSF MRSEC program (DMR-1719875). Technical and facility support provided by the Cornell Energy Systems Institute (CESI) are also gratefully acknowledged.

Notes

The authors declare no competing financial interest.

REFERENCES

(1) Dauxois, T.; Peyrard, M. *Physics of Solitons*; Cambridge University Press: Cambridge, 2006.

(2) Manton, N.; Sutcliffe, P. *Topological Solitons*; Cambridge University Press, 2004.

(3) Heimburg, T.; Jackson, A. D. On Soliton Propagation in Biomembranes and Nerves. *Proc. Natl. Acad. Sci. U.S.A.* **2005**, *102*, 9790−9795.

(4) Appali, R.; Van Rienen, U.; Heimburg, T. A Comparison of the Hodgkin−Huxley Model and the Soliton Theory for the Action Potential in Nerves. *Adv. Planar Lipid Bilayers Liposomes* **2012**, *16*, 275−299.

(5) Andersen, S. S. L.; Jackson, A. D.; Heimburg, T. Towards a Thermodynamic Theory of Nerve Pulse Propagation. *Prog. Neurobiol.* **2009**, *88*, 104−113.

(6) Malomed, B. A.; Mihalache, D.; Wise, F.; Torner, L. Spatiotemporal Optical Solitons. *J. Opt. B Quantum Semiclassical Opt.* **2005**, *7*, R53−R72.
(7) Kartashov, Y. V.; Astrakharchik, G. E.; Malomed, B. A.; Torner, L. Frontiers in Multidimensional Self-Trapping of Nonlinear Fields and Matter. *Nat. Rev. Phys.* **2019**, *1*, 185−197.
(8) Sahin, E.; Blanco-Redondo, A.; Xing, P.; Ng, D. K. T.; Png, C. E.; Tan, D. T. H.; Eggleton, B. J. Bragg Soliton Compression and Fission on CMOS-Compatible Ultra-Silicon-Rich Nitride. *Laser Photon. Rev.* **2019**, *13*, No. 1900114.
(9) Assanto, G.; Peccianti, M. Spatial Solitons in Nematic Liquid Crystals. *IEEE J. Quantum Electron.* **2003**, *39*, 13−21.
(10) Chemnitz, M.; Gebhardt, M.; Gaida, C.; Stutzki, F.; Kobelke, J.; Limpert, J.; Tünnermann, A.; Schmidt, M. A. Hybrid Soliton Dynamics in Liquid-Core Fibres. *Nat. Commun.* **2017**, *8*, No. 42.
(11) Conti, C.; Assanto, G.; Peccianti, M. Nematicons: Optical Spatial Solitons in Nematic Liquid Crystals. *Opt. Photonics News* **2003**, *14*, 44−48.
(12) Leger, L. Observation of Wall Motions in Nematics. *Solid State Commun.* **1972**, *10*, 697−700.
(13) Helfrich, W. Alignment-Inversion Walls in Nematic Liquid Crystals in the Presence of a Magnetic Field. *Phys. Rev. Lett.* **1968**, *21*, No. 1518.
(14) Migler, K. B.; Meyer, R. B. Solitons and Pattern Formation in Liquid Crystals in a Rotating Magnetic Field. *Phys. Rev. Lett.* **1991**, *66*, No. 1485.
(15) Migler, K. B.; Meyer, R. B. Spirals in Liquid Crystals in a Rotating Magnetic Field. *Phys. D* **1994**, *71*, 412−420.
(16) Zheng, C.; Meyer, R. B. Structure and Dynamics of Solitons in a Nematic Liquid Crystal in a Rotating Magnetic Field. *Phys. Rev. E* **1997**, *56*, No. 5553.
(17) Lam, L. Solitons in Liquid Crystals: Recent Developments. *Chaos, Solitons Fractals* **1995**, *5*, 2463−2473.
(18) Brand, H. R.; Fradin, C.; Finn, P. L.; Pesch, W.; Cladis, P. E. Electroconvection in Nematic Liquid Crystals: Comparison between Experimental Results and the Hydrodynamic Model. *Phys. Lett. A* **1997**, *235*, 508−514.
(19) Li, B. X.; Borshch, V.; Xiao, R. L.; Paladugu, S.; Turiv, T.; Shiyanovskii, S. V.; Lavrentovich, O. D. Electrically Driven Three-Dimensional Solitary Waves as Director Bullets in Nematic Liquid Crystals. *Nat. Commun.* **2018**, *9*, No. 1.
(20) Ackerman, P. J.; Trivedi, R. P.; Senyuk, B.; Van De Lagemaat, J.; Smalyukh, I. I. Two-Dimensional Skyrmions and Other Solitonic Structures in Confinement-Frustrated Chiral Nematics. *Phys. Rev. E* **2014**, *90*, No. 012505.
(21) Sohn, H. R. O.; Ackerman, P. J.; Boyle, T. J.; Sheetah, G. H.; Fornberg, B.; Smalyukh, I. I. Dynamics of Topological Solitons, Knotted Streamlines, and Transport of Cargo in Liquid Crystals. *Phys. Rev. E* **2018**, *97*, No. 052701.
(22) Li, B. X.; Xiao, R. L.; Paladugu, S.; Shiyanovskii, S. V.; Lavrentovich, O. D. Three-Dimensional Solitary Waves with Electrically Tunable Direction of Propagation in Nematics. *Nat. Commun.* **2019**, *10*, No. 3749.
(23) Li, B. X.; Xiao, R. L.; Shiyanovskii, S. V.; Lavrentovich, O. D. Soliton-Induced Liquid Crystal Enabled Electrophoresis. *Phys. Rev. Res.* **2020**, *2*, No. 013178.
(24) Shen, Y.; Dierking, I. Dynamics of Electrically Driven Solitons in Nematic and Cholesteric Liquid Crystals. *Commun. Phys.* **2020**, *3*, No. 14.
(25) Nys, I.; Berteloot, B.; Poy, G. Surface Stabilized Topological Solitons in Nematic Liquid Crystals. *Crystals* **2020**, *10*, 840.
(26) Aya, S.; Araoka, F. Kinetics of Motile Solitons in Nematic Liquid Crystals. *Nat. Commun.* **2020**, *11*, No. 3248.
(27) Shen, Y.; Dierking, I. Dynamic Dissipative Solitons in Nematics with Positive Anisotropies. *Soft Matter* **2020**, *16*, 5325−5333.
(28) Shen, Y.; Dierking, I. Electrically Driven Formation and Dynamics of Skyrmionic Solitons in Chiral Nematics. *Phys. Rev. Appl.* **2021**, *15*, No. 054023.
(29) Ackerman, P. J.; Smalyukh, I. I. Static Three-Dimensional Topological Solitons in Fluid Chiral Ferromagnets and Colloids. *Nat. Mater.* **2017**, *16*, 426−432.
(30) Lavrentovich, O. D. Design of Nematic Liquid Crystals to Control Microscale Dynamics. *Liq. Cryst. Rev.* **2020**, *8*, 59−129.
(31) Jeong, J.; Gross, A.; Wei, W. S.; Tu, F.; Lee, D.; Collings, P. J.; Yodh, A. G. Liquid Crystal Janus Emulsion Droplets: Preparation, Tumbling, and Swimming. *Soft Matter* **2015**, *11*, 6747−6754.
(32) Bukusoglu, E.; Pantoja, M. B.; Mushenheim, P. C.; Wang, X.; Abbott, N. L. Design of Responsive and Active (Soft) Materials Using Liquid Crystals. *Annu. Rev. Chem. Biomol. Eng.* **2016**, *7*, 163−196.
(33) Yamamoto, T.; Sano, M. Chirality-Induced Helical Self-Propulsion of Cholesteric Liquid Crystal Droplets. *Soft Matter* **2017**, *13*, 3328−3333.
(34) Nayani, K.; Córdova-Figueroa, U. M.; Abbott, N. L. Steering Active Emulsions with Liquid Crystals. *Langmuir* **2020**, *36*, 6948−6956.
(35) Kim, Y. K.; Wang, X.; Mondkar, P.; Bukusoglu, E.; Abbott, N. L. Self-Reporting and Self-Regulating Liquid Crystals. *Nature* **2018**, *557*, 539−544.
(36) Zhang, R.; Mozaffari, A.; de Pablo, J. J. Autonomous Materials Systems from Active Liquid Crystals. *Nat. Rev. Mater.* **2021**, *6*, 437−453.
(37) Wang, X.; Zhou, Y.; Kim, Y. K.; Tsuei, M.; Yang, Y.; De Pablo, J. J.; Abbott, N. L. Thermally Reconfigurable Janus Droplets with Nematic Liquid Crystalline and Isotropic Perfluorocarbon Oil Compartments. *Soft Matter* **2019**, *15*, 2580−2590.
(38) Wang, X.; Zhou, Y.; Palacio-Betancur, V.; Kim, Y. K.; Delalande, L.; Tsuei, M.; Yang, Y.; De Pablo, J. J.; Abbott, N. L. Reconfigurable Multicompartment Emulsion Drops Formed by Nematic Liquid Crystals and Immiscible Perfluorocarbon Oils. *Langmuir* **2019**, *35*, 16312−16323.
(39) Wang, X.; Zhang, R.; Mozaffari, A.; de Pablo, J. J.; Abbott, N. L. Active Motion of Multiphase Oil Droplets: Emergent Dynamics of Squirmers with Evolving Internal Structure. *Soft Matter* **2021**, *17*, 2985−2993.
(40) de Gennes, P.-G.; Prost, J. *The Physics of Liquid Crystals*; Clarendon Press, 1993.
(41) Gupta, V. K.; Abbott, N. L. Azimuthal Anchoring Transition of Nematic Liquid Crystals on Self-Assembled Monolayers Formed from Odd and Even Alkanethiols. *Phys. Rev. E: Stat. Phys., Plasmas, Fluids, Relat. Interdiscip. Top.* **1996**, *54*, R4540−R4543.
(42) Gupta, V. K.; Abbott, N. L. Uniform Anchoring of Nematic Liquid Crystals on Self-Assembled Monolayers Formed from Alkanethiols on Obliquely Deposited Films of Gold. *Langmuir* **1996**, *12*, 2587−2593.
(43) Gupta, V. K.; Abbott, N. L. Design of Surfaces for Patterned Alignment of Liquid Crystals on Planar and Curved Substrates. *Science* **1997**, *276*, 1533−1536.
(44) Drawhorn, R. A.; Abbott, N. L. Anchoring of Nematic Liquid-Crystals on Self-Assembled Monolayers Formed from Alkanethiols on Semitransparent Films of Gold. *J. Phys. Chem. A* **1995**, *99*, 16511−16515.
(45) Miller, W. J.; Abbott, N. L. Influence of van der Waals Forces from Metallic Substrates on Fluids Supported on Self-Assembled Monolayers Formed from Alkanethiols. *Langmuir* **1997**, *13*, 7106−7114.
(46) Miller, W. J.; Abbott, N. L.; Paul, J. D.; Prentiss, M. G. Planar Anchoring of Nematic 4-n-pentyl-4′-cyanobiphenyl on Self-assembled Monolayers Formed from Alkanethiols on Gold. *Appl. Phys. Lett.* **1996**, *69*, 1852.
(47) Follonier, S.; Miller, W. J. W.; Abbott, N. L.; Knoesen, A. Characterization of the Molecular Orientation of Self-Assembled Monolayers of Alkanethiols on Obliquely Deposited Gold Films by Using Infrared−Visible Sum-Frequency Spectroscopy. *Langmuir* **2003**, *19*, 10501−10509.
(48) Delamarche, E.; Michel, B.; Kang, H.; Gerber, C. Thermal Stability of Self-Assembled Monolayers. *Langmuir* **1994**, *10*, 4103−4108.

https://doi.org/10.1021/acs.langmuir.2c00231
Langmuir 2022, 38, 3575−3584

(49) Kodama, C.; Hayashi, T.; Nozoye, H. Decomposition of Alkanethiols Adsorbed on Au (1 1 1) at Low Temperature. *Appl. Surf. Sci.* **2001**, *169*−*170*, 264−267.
(50) Fukushima, H.; Seki, S.; Nishikawa, T.; Takiguchi, H.; Tamada, K.; Abe, K.; Colorado, R.; Graupe, M.; Shmakova, O. E.; Lee, T. R. Microstructure, Wettability, and Thermal Stability of Semifluorinated Self-Assembled Monolayers (SAMs) on Gold. *J. Phys. Chem. B* **2000**, *104*, 7417−7423.
(51) Cristina, L. J.; Ruano, G.; Salvarezza, R.; Ferrón, J. Thermal Stability of Self-Assembled Monolayers of n-Hexanethiol on Au(111)-(1 × 1) and Au(001)-(1 × 1). *J. Phys. Chem. C* **2017**, *121*, 27894−27904.
(52) Clare, B. H.; Orlando, G.; de Pablo, J. J.; Abbott, N. L. Measurement of the Azimuthal Anchoring Energy of Liquid Crystals in Contact with Oligo(Ethylene Glycol)-Terminated Self-Assembled Monolayers Supported on Obliquely Deposited Gold Films. *Langmuir* **2006**, *22*, 4654−4659.
(53) Skaife, J. J.; Abbott, N. L. Quantitative Characterization of Obliquely Deposited Substrates of Gold by Atomic Force Microscopy: Influence of Substrate Topography on Anchoring of Liquid Crystals. *Chem. Mater.* **1999**, *11*, 612−623.
(54) Widrig, C. A.; Chung, C.; Porter, M. D. The Electrochemical Desorption of N-Alkanethiol Monolayers from Polycrystalline Au and Ag Electrodes. *J. Electroanal. Chem. Interfacial Electrochem.* **1991**, *310*, 335−359.
(55) Pensa, E.; Vericat, C.; Grumelli, D.; Salvarezza, R. C.; Park, S. H.; Longo, G. S.; Szleifer, I.; De Leo, L. P. M. New Insight into the Electrochemical Desorption of Alkanethiol SAMs on Gold. *Phys. Chem. Chem. Phys.* **2012**, *14*, 12355−12367.
(56) Éber, N.; Salamon, P.; Buka Electrically Induced Patterns in Nematics and How to Avoid Them. In *Liquid Crystals Reviews*; Taylor and Francis Ltd, 2016; pp 101−134.
(57) Seo, D. S.; Kobayashi, S.; Nishikawa, M.; Kim, J. H.; Yabe, Y. Odd−Even Effects of the Polar Anchoring Strength in Nematic Liquid Crystal on Rubbed Polyimide Langmuir−Blodgett Films with Alkyl Chain Lengths. *Appl. Phys. Lett.* **1995**, *66*, No. 1334.
(58) Seo, D. S.; Matsuda, H.; Oh-Ide, T.; Kobayashi, S. Alignment of Nematic Liquid Crystal(5CB) on the Treated Substrates: Characterization of Orientation Films, Generation of Pretilt Angles, and Surface Anchoring Strength. *Mol. Cryst. Liq. Cryst.* **1993**, *224*, 13−31.
(59) Faetti, S.; Marianelli, P. Strong Azimuthal Anchoring Energy at a Nematic-Polyimide Interface. *Phys. Rev. E.* **2005**, *72*, No. 051708.
(60) Vilfan, M.; Čopič, M. Azimuthal and Zenithal Anchoring of Nematic Liquid Crystals. *Phys. Rev. E* **2003**, *68*, No. 031704.
(61) Lucchetti, L.; Nava, G.; Barboza, R.; Ciciulla, F.; Bellini, T. Optical Force-Based Detection of Splay and Twist Viscoelasticity of CCN47 across the Nematic-to-Smectic A Transition. *J. Mol. Liq.* **2021**, *329*, No. 115520.
(62) Clare, B. H.; Guzmán, O.; De Pablo, J.; Abbott, N. L. Anchoring Energies of Liquid Crystals Measured on Surfaces Presenting Oligopeptides. *Langmuir* **2006**, *22*, 7776−7782.
(63) Govindaraju, T.; Bertics, P. J.; Raines, R. T.; Abbott, N. L. Using Measurements of Anchoring Energies of Liquid Crystals on Surfaces to Quantify Proteins Captured by Immobilized Ligands. *J. Am. Chem. Soc.* **2007**, *129*, 11223−11231.
(64) Lowe, A. M.; Bertics, P. J.; Abbott, N. L. Quantitative Methods Based on Twisted Nematic Liquid Crystals for Mapping Surfaces Patterned with Bio/Chemical Functionality Relevant to Bioanalytical Assays. *Anal. Chem.* **2008**, *80*, 2637−2645.

https://doi.org/10.1021/acs.langmuir.2c00231
Langmuir 2022, 38, 3575−3584